Effect of Tabor parameter on hysteresis losses during adhesive contact

M. Ciavarella[a], J. A. Greenwood[b], J. R. Barber[c,*]

[a] *CEMEC-Politecnico di Bari, 70125 Bari - Italy.*
[b] *Department of Engineering, University of Cambridge, Cambridge, CB2 1PZ, UK.*
[c] *Department of Mechanical Engineering, University of Michigan, Ann Arbor, MI 48109-2125, U.S.A.*

Abstract

The Tabor p[arameter μ is conventionally assumed to determine the range of applicability of the classical 'JKR' solution for adhesive elastic contact of a sphere and a plane, with the maximum tensile force (the pull-off force) being well predicted for $\mu > 5$. Here we show that the hysteretic energy loss during a contact separation cycle is significantly overestimated by the JKR theory, even at quite large values of μ. This stems from the absence of long-range tensile forces in the JKR theory, which implies that jump into contact is delayed until the separation $\alpha = 0$. We develop an approximate solution based on the use of Greenwood's 'semi-rigid' theory for jump in, and the JKR theory for jump out of contact, and show that for $\mu > 5$, the predicted hysteresis loss is then close to that found by direct numerical solutions using the Lennard-Jones force law. We also show how the same method can be adapted to allow for contact between bodies with finite support stiffness.

Keywords: contact mechanics; hysteresis; adhesion.

1. Introduction

When adhesive forces [e.g. van der Waal's forces] are included in the formulation of an elastic contact problem, the normal loading and unloading curves can be different, implying hysteresis losses during a loading/unloading cycle. This effect is most pronounced in small scale contacting systems such

*jbarber@umich.edu.

as the atomic force microscope [AFM]. In particular, if the AFM is operated in the tapping mode, hysteretic losses will be reflected in a phase shift between the oscillation of the tip and driving excitation [1, 2, 3, 4].

Many analytical treatments of adhesive contact are based on the 'JKR' model [5], in which tensile tractions are allowed within the contact area, the extent of which is then determined by minimizing the total energy, comprised of elastic strain energy, interface energy and potential energy of external forces. This procedure is exactly analogous to the formulation of linear elastic fracture mechanics [LEFM] [6], with the energy release rate here being equated to the interface energy $\Delta\gamma$. This implies a unique value of the mode I stress intensity factor

$$K_I = -\sqrt{2\pi}\lim_{s\to 0} p(s)\sqrt{s} = \sqrt{2E^*\Delta\gamma}\,, \tag{1}$$

where $p(s)$ is the contact pressure at a distance s from the boundary of the contact area and E^* is the composite contact modulus.

Tabor [7] argued that the assumptions of the JKR theory are appropriate for contact between a sphere of radius R and a plane when the 'Tabor parameter'

$$\mu = \frac{1}{\varepsilon}\left(\frac{R(\Delta\gamma)^2}{E^{*\,2}}\right)^{1/3} \tag{2}$$

is sufficiently large, where ε is a length characterizing the range of interaction of the adhesive forces. In particular, Muller *et al.* [8] showed that the maximum possible tensile force (the 'pull-off force') is predicted within a few percent if $\mu > 5$. However, in this paper we shall show that the JKR theory significantly overestimates hysteresis loss, even at quite high values of μ.

2. The JKR equations

The JKR solution for the adhesive contact of a sphere and a plane is conveniently expressed in terms of the dimensionless variables

$$\hat{T} = \frac{T}{R\Delta\gamma}\,; \quad \hat{\alpha} = \frac{\beta^2\alpha}{R}\,; \quad \hat{a} = \frac{\beta a}{R} \tag{3}$$

[9], where T is the applied force (tensile positive), α is the resulting normal separation, a is the radius of the contact area, and β is a dimensionless

parameter defined by

$$\beta = \left(\frac{E^* R}{\Delta\gamma}\right)^{1/3} = \sqrt{\frac{R}{\mu\varepsilon}}\,. \tag{4}$$

With this notation, the force-displacement relation is defined implicitly by the relations

$$\hat{\alpha} = \sqrt{2\pi\hat{a}} - \hat{a}^2\,; \quad \hat{T} = \sqrt{8\pi\hat{a}^3} - \frac{4\hat{a}^3}{3}\,, \tag{5}$$

and is plotted in Fig. 1.

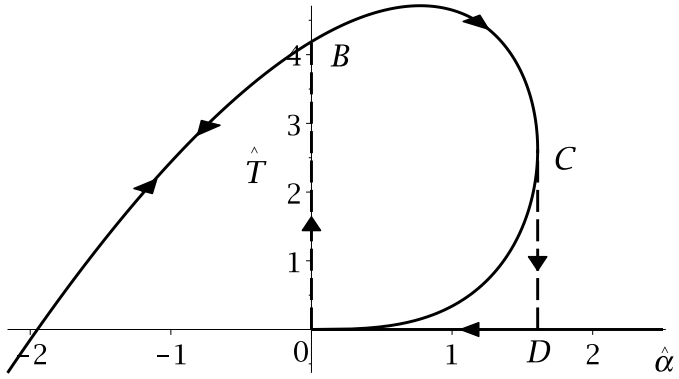

Fig. 1: Loading and unloading of the JKR model.

We can also define a dimensionless measure of the work W done by the force T as

$$\hat{W} \equiv \frac{W}{\mu\varepsilon R\Delta\gamma} = \int \hat{T} d\hat{\alpha} = \int \hat{T}\,\frac{d\hat{\alpha}}{d\hat{a}} d\hat{a} = \frac{8\hat{a}^5}{15} + \pi\hat{a}^2 - \frac{4\sqrt{2\pi\hat{a}^7}}{3}\,, \tag{6}$$

where the final expression is obtained by substituting for $\hat{T}, \hat{\alpha}$ from equations (5) and evaluating the resulting integral. The dimensionless work done in traversing any finite segment of the curve in Fig. 1 can be obtained by imposing appropriate limits on this indefinite integral.

Consider a scenario in which the bodies are initially widely separated, but are caused to approach each other and subsequently separate under displacement control ['rigid grips']. The approach phase must follow the positive

$\hat{\alpha}$-semi-axis as far as the origin, since in the JKR solution no tractions are implied between surfaces with a positive local separation. However, further approach implies an unstable jump into contact at the point B in Fig.1. The force-displacement relation then remains on this branch of the curve until an unstable jump out of contact occurs at point C during the separation phase.

The parameter values at B and C can be determined from equations (5) and the conditions

$$\hat{\alpha}_B = 0 \; ; \quad \left(\frac{d\hat{\alpha}}{d\hat{T}}\right)_C = 0 \; , \tag{7}$$

from which

$$\hat{a}_B = \sqrt[3]{2\pi} \; ; \quad \hat{T}_B = \frac{4\pi}{3} \; ; \quad \hat{\alpha}_C = \frac{3\pi^{2/3}}{4} \; ; \quad \hat{a}_C = \frac{\pi^{1/3}}{2} \; ; \quad \hat{T}_C = \frac{5\pi}{6} \; . \tag{8}$$

The work done by the force T during one approach-separation cycle is defined by the area $OBCDO$ in Fig. 1 and is therefore given by

$$\hat{W}_{JKR} = \left(\frac{8\hat{a}^5}{15} + \pi\hat{a}^2 - \frac{4\sqrt{2\pi\hat{a}^7}}{3}\right)_{\hat{a}_B}^{\hat{a}_C} = 7.092 \; . \tag{9}$$

3. Effect of the Tabor parameter

For lower values of μ, the force-displacement relation is affected by the precise form of the law defining the local relation between the tensile traction σ and the gap h between the surfaces. Analytical solutions can be obtained if this law has a suitably smple form [10, 11], but most authors agree that the force law

$$\sigma(h) = \frac{8\Delta\gamma}{3\varepsilon}\left(\frac{\varepsilon^3}{h^3} - \frac{\varepsilon^9}{h^9}\right) \; , \tag{10}$$

derived from the Lennard Jones 6-12 law for the potential between two molecules [8], is appropriate for van der Waal's interactions. The equilibrium condition ($\sigma = 0$) then occurs at $h = \varepsilon$ and it is usual to assume that compressive contact tractions cause no further reduction in h, so that $\sigma < 0$ implies $h = \varepsilon$.

Several authors [8, 12, 13, 14], have obtained numerical solutions to the adhesive contact problem using the force law (10), a representative dimensionless force-displacement relation for $\mu = 5$ being shown as the red chain

dotted line in Fig. 2. The JKR solution is shown as a black solid line for comparison and confirms that at this value of μ, the pull-off force [i.e. the maximum value of $\hat{T}$] is very close to the JKR value $\hat{T} = 1.5\pi$.

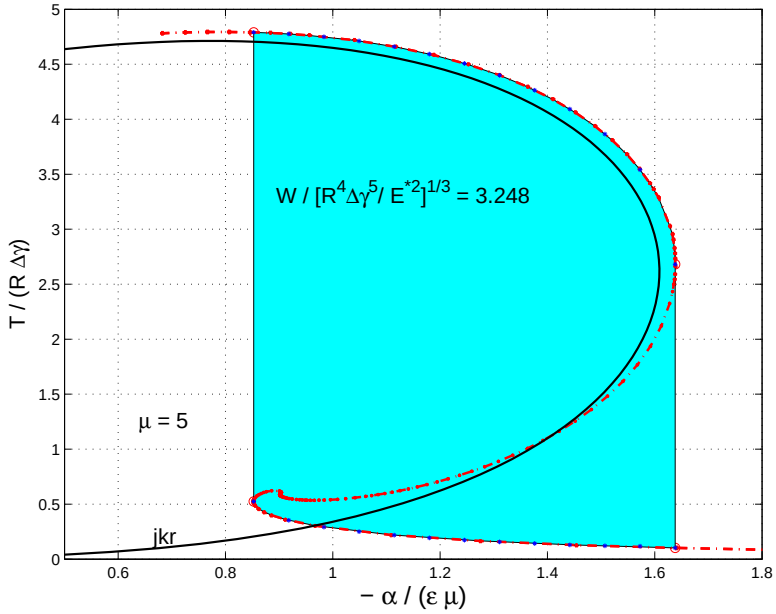

Fig. 2: The dimensionless force-displacement relation for $\mu = 5$.

However, for $\mu = 5$, jump into contact must occur at point A in Fig. 2, and the hysteresis loss is now defined by the shaded area $ABCDA$ between the two branches of the curve. For this value of μ, we obtain $\hat{W} = 3.2482$ which is much lower than the corresponding area (7.092) in the JKR solution, principally because $\hat{\alpha}_A$ at the jump in point A is larger than the value $\hat{\alpha} = 0$ at which jump in is predicted for the JKR solution. More generally, we shall show in the next section that the precise value of $\hat{\alpha}_A$ has a major effect on the hysteresis loss at high values of μ.

3.1. Numerical calculations

Numerical results for the full load-displacement curve [including that shown in Fig. 2] were obtained using the method described by Greenwood [15]. When μ is relatively large, a fine mesh is needed in the radial coordinate, because the tensile tractions are confined to a very thin annulus near the edge of the contact area. However, near the unstable jump-in point A, there is no

contact area and the tractions are everywhere tensile and relatively smooth, so numerical convergence is easy to achieve.

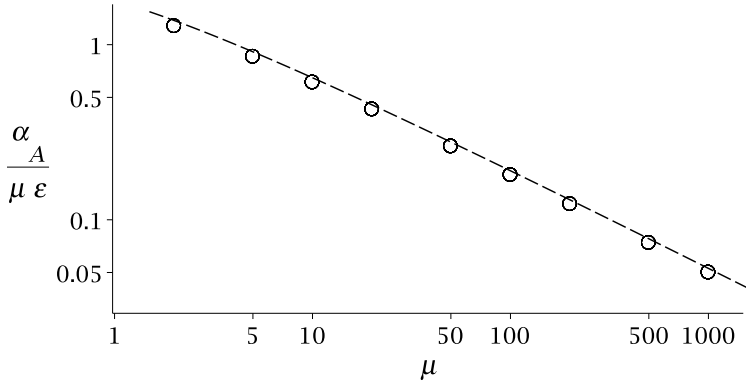

Fig. 3: Separation α at the jump-in point A as a function of the Tabor parameter μ. The circles represent numerical calculations using the Lennard-Jones force law (10), and the line is an approximation obtained from the semi-rigid theory.

The circles in Fig. 3 shows the numerical values obtained for $\hat{\alpha}_A = \beta^2\alpha_A/R = \alpha_A/\mu\varepsilon$ as a function of μ. For large values of μ, a reasonable approximation to the pull-in point can be obtained using Greenwood's 'semi-rigid' theory [15], in which the tractions are determined under the assumption that the bodies remain rigid. The elastic displacements due to these tractions are then determined, and have the effect of increasing the separation between the distant boundaries of the bodies. A similar calculation was performed by Song and Komvopoulos [16], but was then combined with curve fits taken from a finite element analysis.

3.2. The semi-rigid theory

If h_0 is the minimum gap between a rigid sphere a rigid plane, the gap at radius r is $h(r) = h_0 + r^2/2R$ and the attractive force is

$$T = 2\pi \int_0^\infty \sigma\{h(r)\}dr = 2\pi R \int_{h_0}^\infty \sigma(h)dh = \frac{8\pi R\Delta\gamma}{3}\left(\frac{1}{\bar{h}_0^2} - \frac{1}{4\bar{h}_0^8}\right) , \quad (11)$$

or equivalently

$$\hat{T} = \frac{8\pi}{3}\left(\frac{1}{\bar{h}_0^2} - \frac{1}{4\bar{h}_0^8}\right) , \quad (12)$$

where $\bar{h}_0 = h_0/\varepsilon$.

It is important to recall that contact occurs at $h = \varepsilon$ and hence $\bar{h}_0 = 1$, rather than at $h = 0$. Thus, if the bodies were rigid the separation would be defined by $\alpha = h_0 - \varepsilon$. Elastic deformation of the then bodies increases the separation of the distant regions of the bodies.

The elastic displacement at $r = 0$ due to the tractions $\sigma\{h(r)\}$ can be calculated as

$$u(0) = \frac{2}{E^*}\int_0^\infty \sigma\{h(r)\}dr = \pi\varepsilon\sqrt{\frac{2\mu^3}{\bar{h}_0}}\left(\frac{1}{\bar{h}_0^2} - \frac{2145}{4096\bar{h}_0^8}\right) , \tag{13}$$

[15], after which the separation α is estimated as

$$\alpha = h_0 - \varepsilon + u(0) \quad \text{or} \quad \frac{\alpha}{\varepsilon} = \bar{h}_0 - 1 + \pi\sqrt{\frac{2\mu^3}{\bar{h}_0}}\left(\frac{1}{\bar{h}_0^2} - \frac{2145}{4096\bar{h}_0^8}\right) . \tag{14}$$

The pull-in point D can then be determined from the condition

$$\frac{d\alpha}{dT} = \frac{d\alpha}{d\bar{h}_0}\Big/\frac{dT}{d\bar{h}_0} = 0 \quad \text{and hence} \quad \frac{d\alpha}{d\bar{h}_0} = 0 , \tag{15}$$

since $dT/d\bar{h}_0$ is always bounded. Song and Komvopoulos [16] used a finite element model to estimate the value of h_0 at the turning point A, but this calculation can clearly be performed analytically by applying the condition (15) to (14). The resulting relation is plotted parametrically as the dashed line in Fig. 3 and lies quite close to the numerical values over the entire range $\mu > 1$. Also, calculations show that the eighth-power term in equation (14) is completely negligible near α_A for $\mu > 1$, and if this term is dropped, the condition (15) gives the closed-form expression

$$\hat{\alpha}_A \equiv \frac{\alpha_A}{\mu\varepsilon} = \frac{7}{5^{5/7}}\left(\frac{\pi^2}{2}\right)^{1/7}\mu^{-4/7} - \frac{1}{\mu} , \tag{16}$$

which is indistinguishable from the dashed line in Fig. 3. We also note that an excellent curve fit [better than 0.4% accuracy for $\mu > 2$] to the numerical values in this figure can be obtained by multiplying the first term in the expression (17) by 0.95, giving

$$\hat{\alpha}_A = \frac{2.6460}{\mu^{4/7}} - \frac{1}{\mu} , \tag{17}$$

3.3. Hysteresis loss

The numerical solution was used to determine the hysteresis loss in one contact-separation cycle, corresponding [for example] to the shaded area in Fig. 2. Results were obtained for values of μ up to $\mu = 5$ and are shown as circles in Fig. 4. This calculation requires the determination of the force-displacement curve at least up to the point B in Fig. 2 and hence requires an increasingly fine mesh to resolve the region of tensile traction at larger values of μ. However, we shall show in the next section that for $\mu > 5$, we can obtain a good approximation to the hysteresis loss using an analytical approximation.

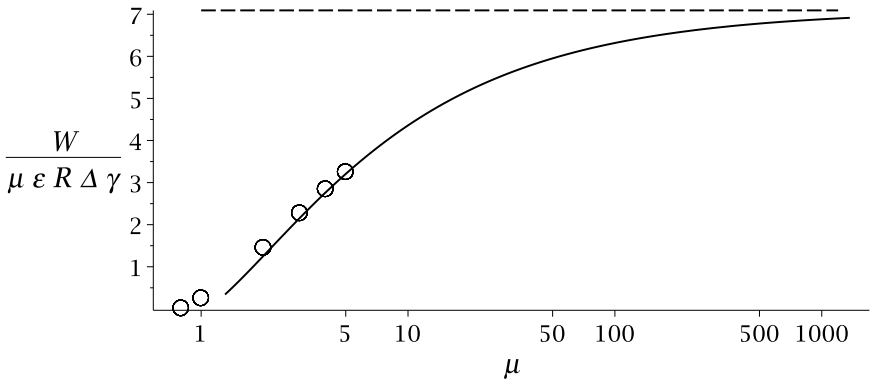

Fig. 4: Dimensionless hysteresis loss $\hat{W}$ determined numerically (circles) and using the 'hybrid' theory (solid line). The horizontal dashed line defines the JKR dissipation from equation (9).

3.4. The 'hybrid' theory

We notice from Fig. 2 that even at $\mu = 5$, the force-displacement curve is quite close to the JKR limit throughout the upper branch, so that an approximation to $\hat{W}$ for finite μ can be obtained by simply replacing the lower limit in equation (9) by $\hat{a}_A$, where

$$\hat{\alpha}_A = \sqrt{2\pi\hat{a}_A} - \hat{a}_A^2 \tag{18}$$

from (5) and $\hat{\alpha}_A$ is given by (17). This necessitates solving the quartic equation (18) for $\sqrt{\hat{a}_A}$, but this presents no serious computational challenge. The resulting relationship is shown as the solid line in Fig. 4, and we note that it is already very close [1.3% error] to the numerical value at $\mu = 5$. As μ is

increased, the force-displacement relation converges on the JKR solution, so this hybrid theory can be expected to improve in accuracy at larger μ.

Fig. 4 shows that the JKR theory [equation (9)] significantly overestimates the hysteresis loss even for large values of μ, the discrepancy being almost entirely due to the effect of μ on the jump-in approach α_A.

3.5. An adhesive length scale

Some insight into the reason that the Tabor parameter fails to characterize the error of the JKR hysteresis prediction can be gained from the analogous field of fracture mechanics, where the appropriateness of the LEFM criterion (1) is conventionally assessed by the 'small-scale yielding' criterion [17]. This argues that the elastic singular field characterizes the conditions at failure, as long as the size of the region in which the stresses exceed the yield criterion is sufficiently small, relative to the other geometric dimensions of the body.

An analogous criterion can be applied to the JKR solution by determining the width s_0 of the region in which the tensile traction $-p(s)$ exceeds the maximum value of the Lennard-Jones traction (10), given by

$$\sigma_0 = \frac{B\Delta\gamma}{\varepsilon} \quad \text{where} \quad B = \frac{16}{9\sqrt{3}} = 1.0264 \approx 1 \; . \tag{19}$$

The stress-intensity factor (1) completely defines the traction field near the edge of the contact, so we can define a universal adhesive length scale s_0 by the equation

$$\sigma_0 = \frac{K_I}{\sqrt{2\pi s_0}} = \sqrt{\frac{E^*\Delta\gamma}{\pi s_0}} \quad \text{or} \quad s_0 = \frac{E^*\Delta\gamma}{\pi\sigma_0^2} = \frac{E^*\varepsilon^2}{\pi\Delta\gamma} \; . \tag{20}$$

We anticipate that the JKR solution will represent a good approximation to an adhesive contact problem if the smallest linear dimension a of the predicted contact area satisfies the condition $s_0 \ll a$. For example, this criterion suggests that the JKR solution will give a good estimate for the pull-off point C in Fig. 1 if $a_C/s_0 \gg 1$. Substituting for a_C from (8) and using (2, 4) to simplify the result, we obtain the criterion

$$\mu^2 \gg \frac{2}{\pi^{4/3}} = 0.44 \tag{21}$$

confirming the appropriateness of μ as a test of the JKR solution near pull-off. However, at the pull-in point, there is no contact region, $a = 0$, and as

we have seen, significant errors are involved even at very high values of μ. We also note that μ contains the radius R and hence can be applied only to the spherical contact problem, whereas the criterion $s_0 \ll a$ can in principle be applied to any contact geometry.

Systems with finite stiffness

The discussion so far is based on the assumption that the contact is achieved under displacement control, which implies an infinitely stiff support system. Clearly this does not apply in any practical case, and for the AFM in particular, the supporting cantilever plays a critical rôle in the hysteretic process. Fortunately, the above calculations are easily modified to allow for a finite support stiffness k if $\mu \gg 1$.

We first note that the separation α is increased by the extension of the spring support, so

$$\hat{\alpha}_S(\hat{T}) = \hat{\alpha}(\hat{T}) + \frac{\hat{T}}{\hat{k}} \quad \text{where} \quad \hat{k} = \frac{\mu\varepsilon k}{R\Delta\gamma} \,, \tag{22}$$

where $\hat{\alpha}(\hat{T})$ is the separation due to the force $\hat{T}$ with an infinitely stiff support. Jump-in and jump-out occur when $d\hat{\alpha}_S/d\hat{T} = 0$ and hence

$$\frac{d\hat{\alpha}}{d\hat{T}} = -\frac{1}{\hat{k}} \,. \tag{23}$$

For $\mu \gg 1$, the jump-out point occurs in a region adequately described by the JKR theory, and hence can be determined from the condition

$$\frac{d\hat{\alpha}}{d\hat{a}} \Big/ \frac{d\hat{T}}{d\hat{a}} = -\frac{1}{\hat{k}} \,, \tag{24}$$

where $\hat{\alpha}, \hat{a}$ are given by equations (5).

For the jump-in point, we can use the semi-rigid theory of Section 3.2, writing

$$\frac{d\hat{\alpha}}{d\bar{h}_0} \Big/ \frac{d\hat{T}}{d\bar{h}_0} = -\frac{1}{\hat{k}} \,, \tag{25}$$

and using equations (12, 14) for $\hat{T}, \alpha$ and noting that $\hat{\alpha} = \alpha/\mu\varepsilon$. However, as we see from Fig. 2, the slope changes very rapidly near A, so the jump-in point is actually very close to $(\hat{\alpha}_A, 0)$, which is given by (17).

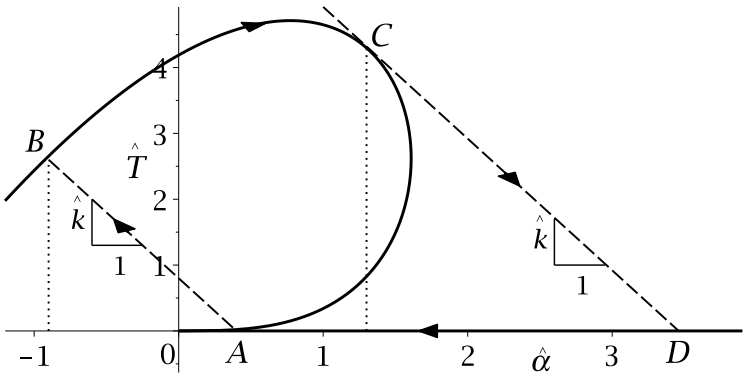

Fig. 5: Loading and unloading path for a system with finite stiffness and $\mu \gg 1$.

With this simplification, the loading-unloading curve will follow the path shown in Fig. 5, with jump-in from A to B and jump-out from C to D. The dimensionless hysteretic loss is given by

$$\hat{W} = \left(\hat{W}(\hat{a}_C) - \hat{W}(\hat{a}_B)\right) + \frac{\hat{T}_C^2 - \hat{T}_B^2}{2\hat{k}} \,, \tag{26}$$

where $\hat{W}(\hat{a})$ is defined by equation (6) and $\hat{a}_B, \hat{T}_B, \hat{a}_C, \hat{T}_C$ are the values of $\hat{a}, \hat{T}$ at points B, C respectively in Fig. 5, both of which lie on the JKR curve defined by equation (5). In this expression, the first term represents the work done by the force $\hat{T}$ in the loading segment from A to B and comprises the area below the curve between the dotted lines in Fig. 5, whilst the second term defines the net energy loss in the spring at jump-in and jump-out. The total hysteresis loss is defined by the area of the region $ABCDA$ in Fig. 5. The rersulting expression is shown as a function of $\hat{k}$ in Fig. 6. As we should expect, the hysteresis loss is asymptotic to the displacement-control limit as $\hat{k} \to \infty$ andit increases as the stiffness $\hat{k}$ is reduced. For $\hat{k} \ll 1$ most of the energy is stored in the spring and the dimensionless hysteresis loss tends to

$$\hat{W} = \frac{\hat{T}_0^2}{2\hat{k}} \,, \tag{27}$$

where $\hat{T}_0 = 3\pi R\Delta\gamma/2$ is the pull-off force in the JKR solution. This expression is shown as the inclined dashed line in Fig. 6.

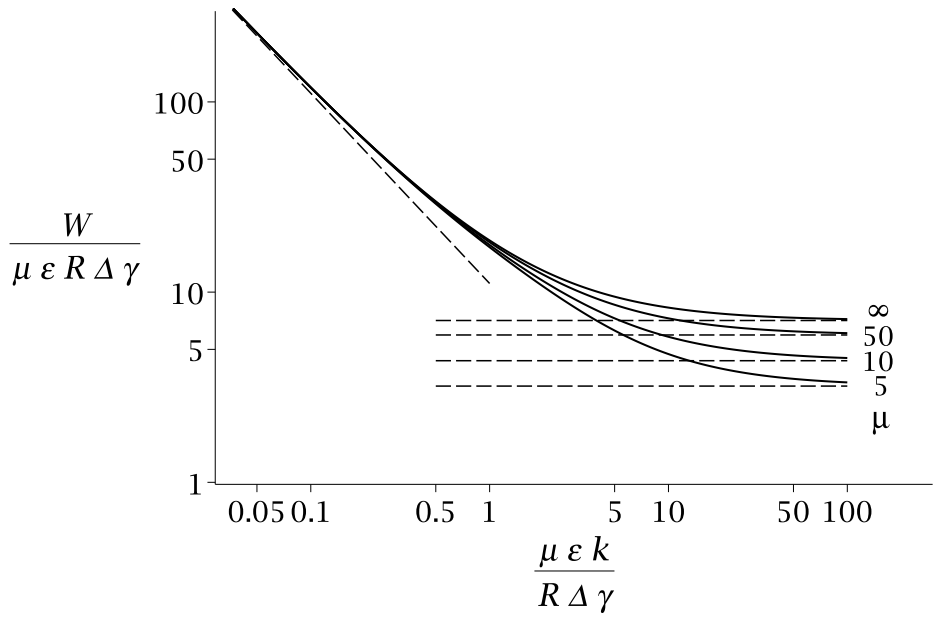

Fig. 6: Hysteresis loss as a function of support stiffness $\hat{k}$ for several values of μ. The inclined dashed line is defined by equation (27) and the horizontal dashed lines represent the displacement-control values taken from Fig. 4.

4. Conclusions

We have shown that the JKR model seriously overestimates the hysteresis energy loss during a contact-separation cycle for a spherical indenter, even at quite high values of the Tabor number μ. In this range, the 'contact' portion of the force-displacement curve is well described by the JKR theory, but jump into contact is not well described, because of the absence from JKR of any interaction before contact. At jump-in the tractions are everywhere tensile, and we find that a good approximation to the force-displacement curve at this point can be obtained using Greenwood's semi-rigid theory [15] in which the elastic displacements are approximated as those due to the tractions between two rigid bodies. Combination of this result with the JKR force-displacement curve for the jump-out condition yields predictions for the hysteresis loss that are very close to a full numerical solution for $\mu > 5$.

The stiffness of the supporting structure has a significant effect on hysteresis and must be taken into account unless the dimensionless stiffness $\hat{k}$ is

large copmpared with unity. However, once again, a combination of a semi-rigid approximation for the jump-in point and the JKR solution for the rest of the force-displacement curve can be expected to give good results for large μ.

References

[1] M. Stark, C. Moller, D. J. Muller, R. Guckenberger, From inages to interactions: High-resolution phase imaging in tapping-mode atomic force microscopy, Biophys. J. 80 (2001) 3009–3018.

[2] A. Noy, C. H. Sanders, D. V. Vezenov, S. S. Wong, C. M. Lieber, Chemically-sensitive imaging in tapping mode by chemical force microscopy: Relationship between phase lag and adhesion, Langmuir 14 (1998) 1508–1511.

[3] J. Tamayo, R. Garcia, Deformation, contact time, and phase contrast in tapping mode scanning force microscopy, Langmuir 12 (1996) 4430–4435.

[4] S. Rutzel, S. I. Lee, R. A, Non-linear dynamics of atomic-force microscope probes driven in lennard-jone potentials, Proc. R. Soc. Lond. 459 (2003) 1925–1948.

[5] K. L. Johnson, K. Kendall, A. D. Roberts, Surface energy and the contact of elastic solids, Proc. R. Soc. Lond. A324 (1971) 301–313.

[6] D. Maugis, M. Barquins, Fracture mechanics and the adherence of viscoelastic bodies, J. Phys. D: Appl. Phys. 11 (1978) 1989–2023.

[7] D. Tabor, Surface forces and surface interactions, J. Colloid Interface Sci. 58 (1977) 2–13.

[8] V. M. Muller, V. S. Yuschenko, B. V. Derjaguin, On the influence of molecular forces on the deformation of an elastic sphere and its sticking to a rigid plane, J. Colloid Interface Sci. 77 (1980) 91–101.

[9] D. Maugis, Contact, Adhesion and Rupture of Elastic Solids, Springer, New York, 2000.

[10] D. Maugis, Adhesion of spheres: The JKR-DMT transition using a Dugdale model, J. Colloid Interface Sci. 150 (1992) 243–269.

[11] J. A. Greenwood, K. L. Johnson, An alternative to the Maugis model of adhesion between elastic spheres, J. Phys. D: Appl. Phys. 31 (1998) 3279–3290.

[12] J. A. Greenwood, Adhesion of elastic spheres, Proc. R. Soc. Lond. A453 (1997) 1277–1297.

[13] J. Q. Feng, Contact behavior of spherical elastic particles: a computational study of particle adhesion and deformations, Colloids & Surfaces 172 (2000) 175–198.

[14] J. Q. Feng, Adhesive contact of elastically deformable spheres: A computational study of pull-off force and contact radius, J. Colloid Interface Sci. 238 (2001) 318–323.

[15] J. A. Greenwood, Adhesion of small spheres, Phil. Mag. 89 (2009) 945–965.

[16] Z. Song, K. Komvopoulos, Adhesive contact of an elastic semiinfinite solid with a rigid rough surface: Strength of adhesion and contact instabilities, Int. J. Solids Structures 51 (2014) 1197–1207.

[17] M. F. Kanninen, C. H. Popelar, Advanced Fracture Mechanics, Clarendon Press, Oxford, 1985.